Direct evidence for coherent low velocity axonal transport of mitochondria

Kyle E. Miller and Michael P. Sheetz

Department of Zoology, Michigan State University, East Lansing, MI 48824

Axonal growth depends on axonal transport. We report the first global analysis of mitochondrial transport during axonal growth and pauses. In the proximal axon, we found that docked mitochondria attached to the cytoskeletal framework that were stationary relative to the substrate and fast axonal transport fully accounted for mitochondrial transport. In the distal axon, we found both fast mitochondrial transport and a coherent slow transport of the mitochondria docked to the axonal framework (low velocity transport [LVT]). LVT was distinct from previously described transport processes; it was coupled with stretching of the axonal framework and, surprisingly, was independent of growth cone advance. Fast mitochondrial transport decreased and LVT increased in a proximodistal gradient along the axon, but together they generated a constant mitochondrial flux. These findings suggest that the viscoelastic stretching/creep of axons caused by tension exerted by the growth cone, with or without advance, is seen as LVT that is followed by compensatory intercalated addition of new mitochondria by fast axonal transport.

Introduction

Neuronal components are primarily synthesized in the cell body (Campenot and Eng, 2000; Goldberg, 2003) and move to supply the growing axon by the classic behaviors of fast and slow axonal transport (Grafstein and Forman, 1980). In most neurons, it is thought that cytoskeletal proteins and organelles are transported by kinesins and dynein along a stationary cytoskeleton (Hirokawa et al., 1997; Brown, 2000) and that elongation occurs by tip growth (Bamburg et al., 1986; for review see Dent and Gertler, 2003). Although there have been numerous studies, both axonal transport and axonal growth (Dent and Gertler, 2003) have been controversial for decades, in part because of significant differences in what seem to be direct observations.

Slow axonal transport was classically envisioned as the movement of a coherent column from the cell body to the growth cone in a process described as axoplasmic flow (Grafstein and Forman, 1980). Today, it is generally accepted that the framework of the cytoskeleton is stationary in cultured chicken dorsal root ganglion (DRG) neurons, as well as in vivo for developing zebrafish and grasshopper neurons (Hirokawa et al., 1997; Brown, 2000). Although an early study suggested that the coherent movement of microtubules may occur in the neurites of PC12 cells (Keith, 1987), later work indicated that the framework of the cytoskeleton was also stationary (Lim et al., 1989). In all but one case, isolated polymers or soluble subunits and organelles are now thought to move along a stationary framework to their site of addition at the growth cone (Brown, 2000; Dent and Gertler, 2003; Ma et al., 2004).

In *X. laevis* neurons, it is agreed that cytoskeletal framework markers move toward the growth cone, but why these neurons seem to have a unique mechanism for axonal transport has been a vexing question (Okabe and Hirokawa, 1992; Chang et al., 1998). Although the reported differences between the outgrowth of *X. laevis* neurons and all other neurons may be real, they may also reflect limitations of methodology. Photobleaching and photoactivation studies are limited by marked regions that dissipate because cytoskeletal polymers are dynamic (Okabe and Hirokawa, 1990). Thus, over prolonged periods of time, uncertainty arises in regard to the position of the mark. Although it has been convincingly demonstrated that marked regions in non–*X. laevis* neurons do not translocate at the rate of growth cone advance (Okabe and Hirokawa, 1990), it is possible that en bloc anterograde movements in all other axons have been overlooked. A more tractable approach to understanding axonal transport is to focus on a component that can be tracked completely. Thus, we have concentrated on mitochondria because they are easily labeled and monitored and move by fast axonal transport, but also form stable associations with the axonal

Correspondence to Kyle E. Miller: kmiller@msu.edu

M.P. Sheetz's present address is Department of Biological Sciences, Columbia University, New York, NY 10027.

Abbreviations used in this paper: DRG, dorsal root ganglion; LVT, low velocity transport.

The online version of this article contains supplemental material.

The Journal of Cell Biology, Vol. 173, No. 3, May 8, 2006 373–381
http://www.jcb.org/cgi/doi/10.1083/jcb.200510097

framework through docking (Wagner et al., 2003; Chada and Hollenbeck, 2004; Miller and Sheetz, 2004).

Mitochondria are critical for neuronal function, and their possible involvement in Alzheimer's disease (Lustbader et al., 2004), Huntington's disease (Bae et al., 2005), and Parkinson's disease (Valente et al., 2004) makes their study clinically relevant. Along the axon, mitochondria alternate between being rapidly transported by motors with instantaneous velocities between ~0.1 and 2 μm/s and docked states where the mitochondria bind actin filaments, neurofilaments, and microtubules (Wagner et al., 2003; Chada and Hollenbeck, 2004; Hollenbeck and Saxton, 2005). Our previous study showed that fast-transported mitochondria stop (dock) along the axon (Miller and Sheetz, 2004). This accounts for the decrease in fast mitochondrial transport along the axon (Morris and Hollenbeck, 1993), but begs the question of how mitochondria are added to the newly elaborated axonal tip.

Although there has been much work on axonal growth, no study has directly observed total transport along the full length of the axon during axonal elongation. To test the current models, we undertook a global study of mitochondrial transport in cultured chicken DRG neurons. Surprisingly, we found that the distal axon was continually being pulled forward, even when the growth cone was stationary, indicating that the axon was under tension that was independent of growth cone movement. These findings indicate that axonal growth in DRG neurons does not occur by tip growth, but rather by axonal stretching caused by a force-generating mechanism in the growth cone, coupled with intercalated addition through fast transport.

Results

Low velocity mitochondrial movement occurs in the distal and middle regions, but not the proximal region, of chicken DRG axons

We investigated mitochondrial transport in chicken DRG neurons grown on polyornithine/laminin-coated coverslips. Our procedure was designed to routinely follow transport and outgrowth for up to 1 h, with an image acquisition rate of 0.5 Hz, while minimizing photodamage (Ligon and Steward, 2000). To facilitate the long term visualization of mitochondrial transport, we (a) reduced the intensity of light used for illumination by using neutral density filters (25 or 50%) and switching the laser to standby mode during observations, (b) used a minimal incubation time and concentration of the MitoTracker CMX-Ros dye (1 min and 100 nM), (c) allowed an interval of several hours (2–4 h) between the time of dye incubation and observation, and (d) observed the neurons in a closed flow chamber to eliminate the accumulation of free radicals (Miller and Sheetz, 2004). Images obtained in this way were assembled into kymographs to reveal en bloc movements that might have been overlooked or discarded by conventional particle-tracking routines or by the photobleaching and photoactivation techniques (Fig. 1, A–D; and Video 1, available at http://www.jcb.org/cgi/content/full/jcb.200510097/DC1). Although the image-capture protocol lowered the optical resolution in regard to submicron mitochondrion morphology, it permits the acquisition of image sequences with excellent temporal resolution and duration.

For our global survey, we analyzed docked mitochondria for movement in the proximal (the first 150 μm continuous with the cell body), middle (the region where neither cell body nor growth cone were in view), and distal axon (the last 150 μm that includes the growth cone). Data were acquired from 2–3-d-old neurons in which the total axonal length exceeded 500 μm. In Fig. 1 E, a total of 19 separate kymographs, each from the axons of different neurons, are assembled to give an overview of the movements of docked mitochondria along the axon. We separated our analysis of observations of the growth cone into periods where the growth cone was either moving forward in the distal region (Fig. 1, E and G) or paused (Fig. 1, F and H) to determine if there was a difference in the pattern of mitochondrial transport.

We found that docked mitochondria move anterogradely, with a low velocity that varies along the axon (Fig. 1 G). Taking the mean velocity of transport for the three regions of the axon revealed a zero velocity in the proximal axon (-2 ± 14 μm/h; mean ± SD; $n = 113$ mitochondria analyzed in eight neurons), an intermediate velocity in the middle of the axon (12 ± 19 μm/h; mean ± SD; $n = 123$ mitochondria analyzed in nine neurons), and the highest velocity in the distal axon (43 ± 26 μm/h; mean ± SD; $n = 80$ mitochondria analyzed in seven neurons; Fig. 1 G). Comparing the mean velocity of transport in the proximal and middle regions of the axon (-2 ± 14 vs. 12 ± 19 μm/h; mean ± SD; $n = 113$ and 123 observations of mitochondrion movement; $P < 0.0001$, two-tailed t test) and the middle and the distal axon during elongation (12 ± 19 vs. 43 ± 26 μm/h; mean ± SD; $n = 123$ and 80 observations of mitochondrion movement; $P < 0.0001$, two-tailed t test) revealed that the low velocity movements of the mitochondria significantly increased in rate along the length of the axon.

Low velocity mitochondrial movement occurs during growth cone pauses

If low velocity movement of docked mitochondria occurred during growth cone pauses, it would indicate that it occurred as the result of a transport process, instead of axonal stretching through growth cone advance. We found that, in the distal axon, low velocity transport (LVT) continued unabated during pauses (Fig. 1, F and H; 42 μm/h ± 23; mean ± SD; $n = 65$ mitochondria from nine different neurons for the movement of docked mitochondria during growth cone pauses vs. 43 ± 26 μm/h; mean ± SD; $n = 80$ mitochondria analyzed in seven neurons for the movement of docked mitochondria during growth cone advance; $P = 0.66$ from a two-tailed t test comparing the mean velocity of transport over the last 120 μm of the distal axon for advancing and paused growth cones, but excluding the last 10 μm of the axon for paused growth cones). Thus, the low velocity movements of the mitochondria occur through a transport mechanism that is independent of growth cone advance.

Correlation analysis of back-and-forth movements suggests mitochondria interact with a common underlying axonal framework

Although LVT was independent of growth cone advance Fig. 1, F and H), it raised the question of whether the movements of the

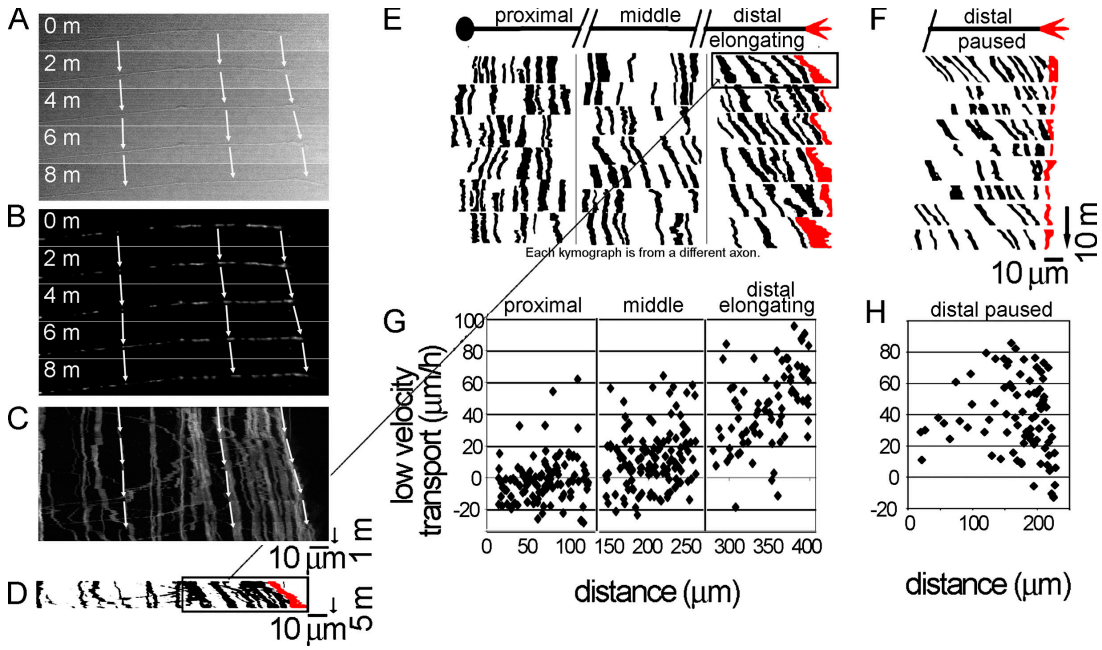

Figure 1. **Low velocity mitochondrial transport increases along the axon and continues during growth cone pauses.** (A) Axonal morphology at the light level during outgrowth. The growth cone is toward the right hand side (Video 1). (B) Mitochondrial distribution during outgrowth. The arrows show the change in position of three different mitochondria over time. (C) The kymograph gives a complete overview of mitochondrial transport, and (D) the color-inverted time-compressed kymograph better illustrates low velocity movements. The position of the most distal mitochondria in the growth cone are highlighted in red. (E) A montage of multiple individual kymographs illustrating low velocity mitochondrial transport from the proximal, middle, and distal regions of the axon during axonal elongation. 19 kymographs from different neurons are shown, and the corresponding kymograph in D is found at the top right-hand side in E. (F) Kymographs illustrating low velocity mitochondrial transport in the distal axon during growth cone pauses. Nine kymographs from different axons where the growth cones were paused are shown. (G) Quantification of LVT in the proximal, middle, and distal axon during axonal elongation demonstrates that it increases along the axon. The slopes of the lines from the kymographs were used to estimate the velocity of transport in different regions of the axon. Data points are the velocities of individual docked mitochondria. Although the length scale is continuous along the bottom of the graph, the measurements are a composite of different axonal regions. (H) Quantification of LVT in the distal axon during growth cone pauses demonstrates that it continues unabated. Video 1 is available at http://www.jcb.org/cgi/content/full/jcb.200510097/DC1.

docked mitochondria reflected the coherent movement of the axonal framework or were moving via an asynchronous transport mechanism powered by motors moving individual cargoes in a stop-and-go manner. For example, the apparent low velocity movements could result from the coherent movement of the underlying axonal framework (Okabe and Hirokawa, 1992; Chang et al., 1998). Alternatively, they could result from asynchronous mitochondrion transport by an unidentified slow kinesin or myosin, or from interaction with cytoskeletal filaments (Reinsch et al., 1991; Wagner et al., 2003; Chada and Hollenbeck, 2004) undergoing brief, short-distance stop-and-go transport (Baas, 1997; Brown, 2000). To differentiate between these two modes, we analyzed the correlation between the changes in mitochondrial position over time (i.e., the first derivative) along the axon (Fig. 2). A high correlation would suggest movement of the axonal framework, but the lack of a correlation would suggest asynchronous transport. This test was more stringent than a simple correlation because it tested whether small back-and-forth movements were linked (Fig. 2 C), rather than occurring asynchronously, yet in the same overall direction. Mitochondrial positions from thresholded montages were determined in ImageJ using the Analyze Particles function. The coordinates of the positions were then smoothed using a running 30-s average (Fig. 2 B). The change in position over 1-min intervals was calculated (Fig. 2 C) to examine the correlation between the movements of the mitochondria with each other (Fig. 2 D). Movements of mitochondria along the axon shaft were highly correlated ($r^2 = 0.51$; $P < 0.0001$; $n = 62$; five separate pairs of mitochondria were analyzed; Fig. 2 D for a representative example). Surprisingly, there was a much smaller correlation between the movement of mitochondrion in the growth cone and the axonal mitochondrion ($r^2 = 0.08$; $P = 0.03$; $n = 62$; Fig. 2 E). This low correlation appeared to occur because LVT of the mitochondria along the axon persisted during growth cone pauses, yet phases of growth cone advance occurred more rapidly than LVT. The last 10 min of the kymograph in Fig. 2 A and Video 2 (available at http://www.jcb.org/cgi/content/full/jcb.200510097/DC1) demonstrate transport during a growth cone pause, and the time period between 35 and 50 min shows a rapid advance of the growth cone that is faster than LVT. These results demonstrate that LVT of docked mitochondria occurs because they interact with a coherent framework that is in motion, but that this motion is not tightly linked to growth cone motility.

Changes in intermitochondrial distance suggests that low velocity mitochondrial transport is caused by stretching of the axon

To test if stretching similar to that reported in *X. laevis* neurons occurred, we examined how the distance between pairs of

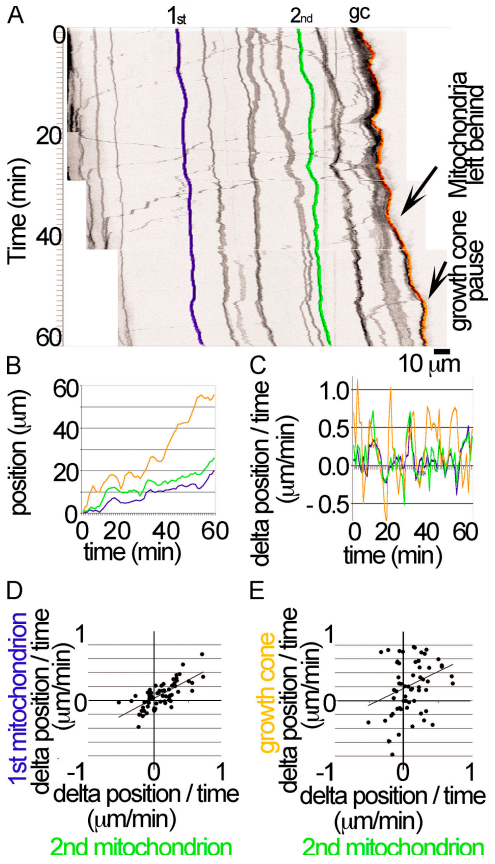

Figure 2. **Low velocity mitochondrial movements are highly correlated along the axon.** (A) High resolution kymograph of mitochondrial transport from a single neuron followed for 1 h, with frames acquired every 2 s. Translucent colored lines illustrate the positions of two mitochondria along the axon and the most distal mitochondrion in the growth cone. Examples where the growth cone advances rapidly, leaving mitochondria from the growth cone behind in the axon shaft and a growth cone pause, are pointed out with arrows to illustrate that LVT is not tightly linked to growth cone advance (Video 2). (B) The relative positions over time of two mitochondria along the axon and the most distal mitochondria in the growth cone. The positions of the three mitochondria highlighted in A are shown, with the initial positions of the mitochondria centered at the origin. (C) Change in mitochondrial position over time. A rolling 30-s average of position was used to smooth the data, and then the minute-to-minute change in the position of the mitochondria was determined for the correlation analysis (n = 62 points). (D) Back-and-forth movements of docked mitochondria along the axon shaft are highly correlated. This is a plot showing the relative minute-to-minute change in the positions of two mitochondria along the axon shaft (r^2 = 0.51; n = 62; $P < 0.001$). (E) Movements of mitochondria in the growth cone are less correlated with movements of mitochondria along the axon. This is a plot showing the minute-to-minute change in the position of a mitochondrion along the axon shaft and a mitochondrion in the growth cone (r^2 = 0.08; n = 62; P = 0.03). Video 2 is available at http://www.jcb.org/cgi/content/full/jcb.200510097/DC1.

mitochondria changed over time. We analyzed the distances between 166 consecutive pairs of docked mitochondria from nine different axons over 10–15 min time periods in the distal axons where the growth cone was elongating. Using a two-tailed t test between the observed mean and a hypothesized population with a mean of zero (Zar, 1999), we found that the spacing between the mitochondria over the last 150 μm of the axon increased significantly, at a rate of 0.8 ± 0.7% per minute (mean ± SD; $P < 0.005$, against the null hypothesis that the distance between

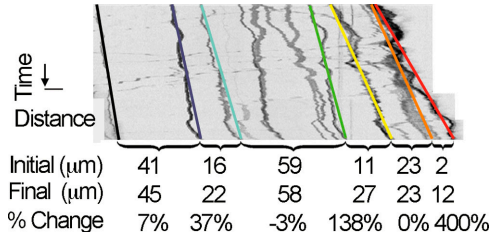

Figure 3. **Intermitochondrial distances increase during axonal elongation.** A kymograph with lines drawn from the initial to the final points of mitochondrial position over a 1-h period. The time arrow is equal to 10 min and the distance bar is 10 μm. Increases between mitochondrial pairs are most prominent near the growth cone (Video 2). The increases in intermitochondrial distance are consistent with axonal stretching. Video 2 is available at http://www.jcb.org/cgi/content/full/jcb.200510097/DC1.

the mitochondria is constant). The SD was large because there was a variation in displacement along the axon (see example in Fig. 3 and Video 2). In the proximal axon, we found that the rate of spacing change was 0.004 ± 0.025% per minute (n = 138 consecutive pairs from 11 different neurons). This was not significantly different from a 0% rate of change. These results suggested that low velocity mitochondrial transport occurred by a process similar to axonal stretching reported in *X. laevis* neurons, but differed in that it only occurred distally (Okabe and Hirokawa, 1992; Chang et al., 1998).

LVT is independent of growth cone advance

Although we found clear evidence for LVT of docked mitochondria during growth cone pauses over 10–15 min time intervals, this movement could have been caused by a passive, time-delayed elastic property of the axon that abated over time (Dennerll et al., 1989). Although in most cases pauses were relatively brief, in three examples we observed growth cones that remained paused for >30 min (see Fig. 4 A for individual frames from a time-lapse movie that lasted 50 min, with the accompanying kymograph in Fig. 4 B, and Video 3, available at http://www.jcb.org/cgi/content/full/jcb.200510097/DC1). In this example, LVT continued after the growth cone paused, and even increased in velocity (a similar example of this type of increase was found in the last 10 min of the kymograph in Fig. 2). This provided strong and direct evidence that low velocity mitochondrial transport in the absence of growth cone advance was not a passive, time-delayed viscoelastic response caused by the advance of the growth cone, but a transport process.

Fast mitochondrial transport decreases along the axon

Fast transport has been considered the sole mechanism for moving mitochondria along the axon. Our findings suggest that it works in concert with LVT. To determine the pattern and flux of fast mitochondrial transport, we measured the flux by counting the mitochondria per hour that passed a single point in the center of kymographs from the proximal (n = 132 mitochondria from 10 neurons), middle (n = 102 mitochondria from nine neurons), and distal (n = 91 mitochondria from 13 neurons; pooled data; see next paragraph for advancing vs. paused growth

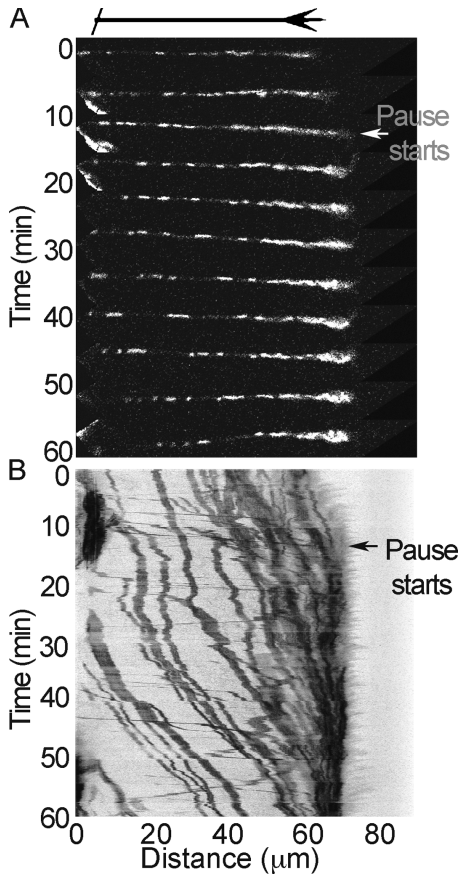

Figure 4. **LVT is independent from growth cone advance.** (A) Montage of the individual frames of a time-lapse movie, showing the distribution of mitochondria along the distal axon during a prolonged growth cone pause. The growth cone is toward the right side of the kymograph and the scale is across the bottom of B. During the first 10 min the growth cone is advancing. It then stops and remains paused for the next 50 min (Video 3). (B) Kymograph to facilitate the visualization of LVT. After the growth cone pause, LVT continues without decreasing in velocity. Video 3 is available at http://www.jcb.org/cgi/content/full/jcb.200510097/DC1.

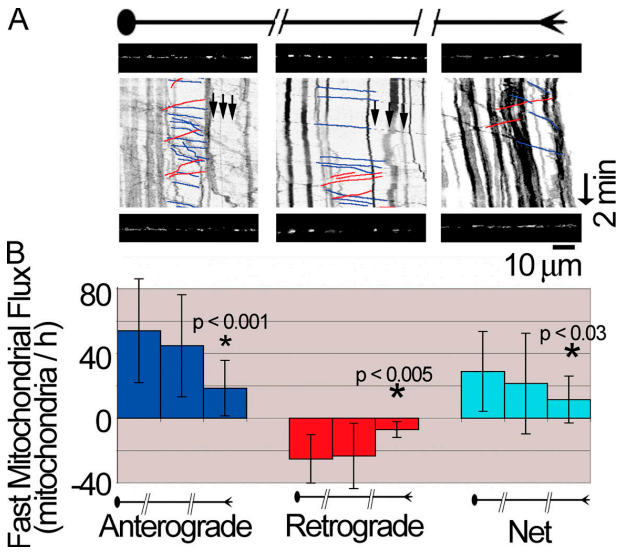

Figure 5. **Fast mitochondrial flux decreases along the axon.** (A) Kymographs from the proximal, middle, and distal regions of the axon during periods of elongation. Frames from the beginning and end of the movie showing the distribution of the mitochondria are found above and below the kymographs. The black lines are the traces of the mitochondria, with the more vertical lines reflecting the positions of mitochondria that are either stationary or undergoing LVT. The blue and red lines are hand-drawn traces reflecting anterograde and retrograde fast mitochondrial transport, respectively. Arrows point to examples of individual fast-transported mitochondria. The growth cone is toward the right side of the kymographs, and the initial time points are at the top. (B) Quantitative analysis of fast transport in the three regions of the axon demonstrates that anterograde, retrograde, and net mitochondrial transport decrease along the axon (*n* is from 10, 9, and 13 neurons for the proximal, middle, and distal regions of the axon, respectively). The error bars are the mean ± SD. Significance levels are for the difference between the levels of transport between the proximal and distal axonal regions as calculated using a two-tailed *t* test. Along the axon, fast mitochondrial transport declines.

cone breakdown) regions, at a rate of >0.2 μm/s (Fig. 5 A). Significant decreases in flux occurred between the proximal and distal regions for anterograde, retrograde, and net transport (Fig. 5 B). Globally, the number of fast-transported mitochondria was highest in the proximal axon and decreased significantly in the distal axon.

When we examined fast transport during growth cone pauses, we found no significant differences in the flux in the distal axon between periods of axonal elongation and growth cone pauses for either anterograde (22 ± 16 vs. 18 ± 15 mitochondria/h; mean ± SD; $n = 7$ mitochondria from six neurons; $P = 0.39$) or retrograde fast transport (7 ± 5 vs. 9 ± 5 mitochondria/h; mean ± SD; $n = 7$ mitochondria from six neurons; $P = 0.43$). Although changes in fast mitochondrial transport have been linked to changes in axonal outgrowth (Morris and Hollenbeck, 1993), our findings suggest fast mitochondrial transport is handled differentially during brief pauses seen during normal outgrowth. These results indicated that fast mitochondrial flux decreased along the axon, but raised the question of the relative contributions of fast flux and LVT to total mitochondrial flux.

Fast and low velocity mitochondrial transport act reciprocally to generate a constant flux along the axon

To determine the relative contributions of fast flux and LVT, we converted velocity to flux (mitochondria/h) by multiplying the rate of LVT (μm/h) by mitochondrial density (mitochondria/μm). Mitochondrial density was determined by counting the total mitochondrial number along measured lengths in the proximal, middle, and distal axon (Miller and Sheetz, 2004). In each region, 10 axons were analyzed, and 849 mitochondria were counted in total. The densities of the mitochondria in the proximal, middle, and distal axon were 0.34 ± 0.11 (mean ± SD), 0.22 ± 0.07, and 0.27 ± 0.10 mitochondria/μm, respectively. Along the axon, our analysis demonstrated that flux from fast transport decreased, flux from LVT increased, and net flux was relatively constant (Fig. 6). Although this analysis did not allow an absolute measure of the contributions of the different modes of transport at each point along the axon, it provided a comparison that strongly suggested a model where fast transport and LVT worked together to transport mitochondria at a constant flux during axonal elongation (Fig. 6).

Discussion

These observations show that docked mitochondria in the distal axon slowly move anterogradely by a LVT process, and that the velocity increases as the mitochondria approach the growth cone (Fig. 1). This transport occurs both during periods of axonal elaboration and during growth cone pauses (Figs. 1 and 4). Correlation analysis indicates that LVT occurs because docked mitochondria interact with a coherent axonal framework that is slowly transported toward the growth cone (Fig. 2). These movements are linked to increases in the intermitochondrial distance in the distal axon, which suggests that low velocity mitochondrial transport occurs through a conserved mechanism similar to that seen in *X. laevis* neurons (Fig. 3). Analysis demonstrates that LVT, in combination with fast axonal transport, generates a constant flux along the axon during elongation (Figs. 1, 5, and 6). We suggest that the axonal framework is transported at a low velocity in the distal axons of cultured DRG neurons by a force-generating mechanism that is independent of growth cone advance.

In *X. laevis* neurons, marks on microtubules and granules attached to the surface of the axon translocate coherently with a velocity profile that increases along the axon (Reinsch et al., 1991; Popov et al., 1993). Because docked mitochondria are coherently transported along the axon with an increasing velocity profile that is distally associated with increases in the distances between pairs of docked mitochondria (Figs. 1–3), we suggest that frog and chick neurons have similar mechanisms for axonal outgrowth.

These results are consistent with stretching of the axonal shaft, but because they occur independently of growth cone advance they reflect transport (Figs. 1 and 4). Although this is en bloc transport of the cytoskeletal framework (Fig. 2) and may contribute to slow axonal transport because it does not occur in the proximal axon (Fig. 1; Lasek et al., 1984), it cannot entirely account for slow axonal transport (Campenot et al., 1996). To convey the notion that the movement we observe reflects transport, but is not slow axonal transport, we suggested calling the phenomena LVT.

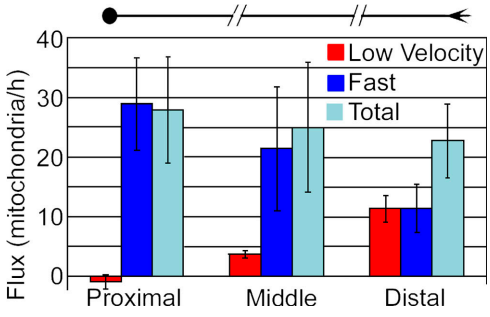

Figure 6. **Fast and low velocity mitochondrial transport act reciprocally to generate a constant flux along the axon.** LVT (from Fig. 1) was converted to low velocity flux based on the density of mitochondria along the axon, as described in the text. The total fluxes are the sums of contributions made by fast transport and LVT in each region of the axon. For each column, the mean ± the SEM is shown. For total fluxes, the error bars are equal to the sums of the SEMs for fast and velocity transport. Total flux in each region is relatively constant along the axon because of the reciprocal contributions of fast and LVT.

Although our conclusions differ from those of previous work, those studies focused on the middle or proximal axon, and did not rule out distal LVT. For example, Lim et al. (1990) demonstrated conclusively that photobleached marks in the proximal axon of cultured rat DRG neurons were stationary. Ruthel and Hollenbeck (2003) demonstrated that axonal towing did not pull mitochondria from the cell bodies of neurons. We previously reported (Miller and Joshi, 1996) that labeled microtubules in the cell body were not transported into axons. Okabe and Hirokawa (1990) demonstrated that photobleached and activated marks along rat DRG axons did not advance at a speed equal to the rate of growth cone advance. Thus, this study and previous works differ in their conclusions, but their results are in agreement.

Our results are also consistent with earlier findings that tension leads to en bloc viscoelastic displacement of the internal cytoskeletal framework (Suter et al., 1998). When ligand-coated beads are held on the surface of stationary growth cones, internally generated tension results in viscoelastic displacement of organelles and microtubules (Suter et al., 1998). When this tension is experimentally relaxed, the initial surge of microtubules and organelles recover their original position (Suter et al., 1998). Our results extend these observations in two ways. First, they demonstrate that a force-generating mechanism leads to movements not only in the growth cone but also along the axonal framework (Figs. 1–4; Suter et al., 1998). Second, they show that force generation in the growth cone occurs during both growth cone advances and pauses (Figs. 1 and 4; Halloran and Kalil, 1994).

Force generation in the growth cone has been widely attributed to a myosin/actin-dependent process (Jay, 2000; Brown and Bridgman, 2003). Although a myosin/actin-linked clutch may be engaged during axonal elaboration and disengaged during growth cone pauses (Mitchison and Kirschner, 1988; Jay, 2000; Suter and Forscher, 2000; Jurado et al., 2005), we suggest the clutch for LVT is always activated during growth cone–mediated axonal elongation. This is consistent with the observation that myosin/actin-dependent activities are important for force generation, but are not absolutely required for axonal elaboration (Joshi et al., 1985; Spero and Roisen, 1985; Letourneau et al., 1987; Bridgman et al., 2001).

Although we have focused on mitochondria, based on the correlation analysis (Fig. 2) it seems likely that the phenomena of LVT includes the movement of a coherent cytoskeletal framework. The observation of LVT in the distal, but not the proximal, axon suggests that forces generated in the growth cone are dissipated along the axon through transmembrane contacts with the substrate (Chang et al., 1998). Furthermore, LVT velocity would be expected to increase distally simply because there is more space/opportunity for material to have been added behind increasingly distal markers (Popov et al., 1993). Although this intuitively suggests a pushing mechanism, previous evidence indicates that application of tension at the growth cone leads to axonal lengthening and microtubule assembly (Bray, 1984; Lamoureux et al., 1989; Zheng et al., 1993). If microtubule

assembly along the axon drove LVT by pushing forces, it would be expected that the induction of microtubule assembly would lead to a lengthening of the axon. Instead, it is found that microtubule assembly by treatment with taxol slows elongation and increases axonal caliber (Letourneau and Ressler, 1984; Letourneau et al., 1986). Thus, we suggest that viscoelastic stretching, instead of pushing by motors or assembly, drives axonal elongation (Fig. 7).

If stretching of the axon occurred without mass addition, the axon would thin and eventually break. Although we did not measure axonal diameter during elongation, two recent studies suggest that substantial lengthening without thinning occurs in response to tension-induced elongation. In one experiment, the internodal spacing between the nodes of Ranvier in rat sciatic nerve was measured after orthopedic leg-lengthening procedures. They found that doubling the length of the nerve doubled the internodal distance without a significant decrease in axonal diameter (Abe et al., 2004). In the second experiment, tension-induced lengthening of the axon at rates of up to 8 mm/day for 20 d occurred with a concomitant 35% increase in axonal diameter (Pfister et al., 2004). Although older work suggested that axonal stretching in *X. laevis* neurons is not real growth because the axonal diameter thins (Okabe and Hirokawa, 1992; Popov et al., 1993), these more recent studies (Abe et al., 2004; Pfister et al., 2004) suggest that tension-induced lengthening of the axon is compensated over longer times by mass addition along the axon. Based on observations of mitochondrial docking along the axon (Chada and Hollenbeck, 2004; Miller and Sheetz, 2004) and the proximal to distal decline in fast mitochondria transport (Fig. 5; Morris and Hollenbeck, 1993), we suggest that new mitochondria are added by docking (Miller and Sheetz, 2004) to compensate for gaps created by axonal stretching. Thus, we suggest tension generated at the growth cone leads to axonal elongation and then intercalated mass addition (Fig. 7).

Our calculations indicate that there is a constant total flux of mitochondria along the axon, which may be important for maintaining a constant mitochondrial distribution over space and time during elongation. When the rate of flux varies, we suggest that addition occurs where flux slows (Miller and Samuels, 1997) and depletion occurs where flux increases. The simultaneous large increase in LVT associated with stretching and the drop in fast mitochondria flux in the distal axon (Fig. 6) is consistent with this region as the primary site of viscoelastic axonal stretching/creep and intercalated addition. As the pool of fast-transported mitochondria moves along the axon, flux would be expected to decrease because mitochondria dock in the gaps created during LVT and to replace damaged mitochondria (Miller and Samuels, 1997; Chada and Hollenbeck, 2004; Miller and Sheetz, 2004). This model of axonal growth (Fig. 7) simultaneously explains the increasing flux profile of LVT (Fig. 1 G and Fig. 7 B) and the decrease in fast anterograde mitochondrial transport (Fig. 5 and Fig. 7 C).

As we and others have observed, axonal elaboration occurs by a process where components that have accumulated in the growth cone are consolidated in the axonal shaft (Fig. 2 and Video 2; Dent and Gertler, 2003). Based on our observations that mitochondria undergoing LVT slow down as they enter the

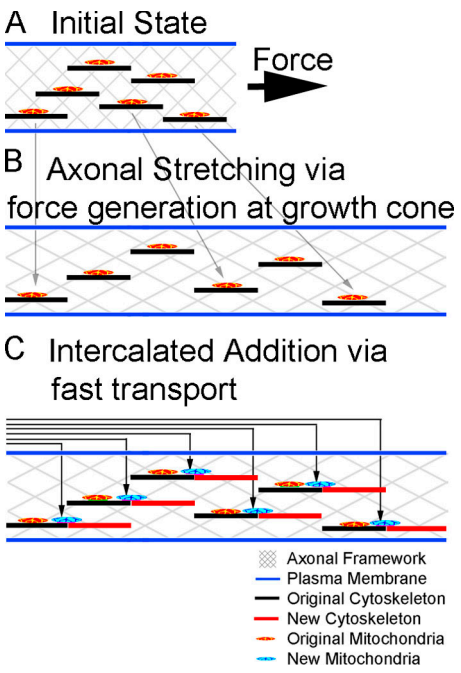

Figure 7. **Axonal growth by LVT and intercalated addition.** (A) Docked mitochondria and cytoskeletal elements are embedded in the axonal framework. (B) Tension generated by forces at the growth cone leads to viscoelastic stretching/creep and an initial decrease in the density of cytosolic components. LVT, as indicated by the gray arrows, is occurring with a flux profile that increases along the axon. (C) Intercalated addition by fast transport restores cytosolic density. Fast flux, as indicated by the arrows, deposits mitochondria in an intercalated fashion and decreases along the axon.

growth cone during growth cone pauses (Fig. 1 H and Fig. 4 B), we speculate that the motor complex generates pulling forces on the axonal shaft and pushing or contractile forces in the growth cone. Over time, the process of elaboration appears to involve periods of protrusion and engorgement, as is generally accepted (Dent and Gertler, 2003); however, our work indicates that both fast axonal transport and LVT move cytosolic components into the growth cone.

As a speculative hypothesis for axonal elongation in terms of LVT, we propose that tension generation at the growth cone, with or without advance, leads to low velocity mitochondrial transport through viscoelastic stretching/creep of the axonal framework. The axonal thinning caused by viscoelastic stretching is then compensated for by intercalated addition of mitochondria and other cytosolic components (Fig. 7).

In summary, in most growing neurons it is thought that the axonal framework is stationary. Our data show that in growing chick DRG neurons the axonal framework undergoes a LVT. This transport increases in velocity along the axon, is associated with viscoelastic stretching, and is independent of growth cone movement. Furthermore, low velocity stretching and fast axonal transport are reciprocally related such that there is a constant flux of mitochondria along a growing axon. We suggest that axonal growth occurs by stretching of the axon through a LVT that is independent of growth cone advance, followed by the intercalated addition of material delivered by fast axonal transport.

Materials and methods

Cell culture and fluorescent dyes

The methods and equipment used were previously described (Miller and Sheetz, 2004). Images were acquired on a confocal system (FV300 FluoView; Olympus) with built-in photomultiplier tubes on a microscope body (model IX70; Olympus) using the FluoView acquisition software, and a 60×, 1.4 NA, PlanApo objective (Olympus). Samples were illuminated with an argon/krypton Omnichrome 488/568/647 line laser set to standby mode, with the laser intensity set at 6%, the confocal aperture set at 5, and pixel dwell times of either 100 or 200 μs; the light was further attenuated with neutral density filters (either 25 or 50%). Cells were observed in an enclosed flow chamber in DME with high glucose, L-glutamine, and pyridoxine HCl, and without sodium pyruvate (Invitrogen) that was then supplemented with 10% fetal calf serum, 10 ng/ml^{-1} nerve growth factor (Sigma-Aldrich), and 1 mM sodium pyruvate. Temperature was maintained at 37°C using a forced air heater. Embryonic day 14 chicken DRG neurons grown on poly-L-ornithine/laminin coated glass coverslips were cultured and used either 2 or 3 d after plating. Mitochondria were labeled with 0.1 μM MitoTracker red CMX-Ros (Invitrogen) in DME for 1 min, and then allowed to recover for at least 2 h in fresh media.

Image acquisition

After extensive analysis of mitochondrial movements in axons, we developed a method to capture their movements in kymograph form. This procedure was better than single particle tracking because it avoided the manual analysis of collision events, which confound current tracking routines, and it provided a complete view of all of the mitochondrial movements (both low and fast velocity) in one figure.

For the creation of kymographs, FluoView files were opened in ImageJ software (National Institutes of Health [NIH]) as stacks, rotated so that the axons in the images were horizontal, cropped, and resliced to switch the time axis and the y axis. These stacks were then z-projected using the Standard Deviation option, which resulted in 32-bit images, with time located on the y axis and distance on the x axis. The kymographs were then converted to 16 bits and saved. For analysis of low velocity movements (Fig. 1 E), raw kymographs were opened in Photoshop (Adobe), levels were adjusted to maximize bit depth, and images were converted to 8 bits, inverted in color, compressed fivefold on the time axis, thresholded using the Filter/Sketch/Photocopy function, and thresholded using the standard function (Image:Adjustments:Threshold). Compression of the image on the time axis, followed by thresholding, erased most of the fast-transport mitochondria. Any traces of fast-transported mitochondria and noise were erased by hand so that each docked mitochondria was an individual trace (Fig. 1, inset). These images were overlaid with the original kymographs to verify that they accurately reflected the low velocity movements of the mitochondria. The images were saved as uncompressed 8-bit tiff files. For the analysis of velocity, images were opened in ImageJ or NIH image. To determine the angle (velocity) and position of each mitochondrial trace, we used the analyze particle function (Analyze: Analyze Particle). The results were exported to Excel (Microsoft) and converted to velocities.

For the analysis of fast mitochondrial transport, a single position in the center of the axon was picked and a line was drawn along the time axis of unfiltered unthresholded kymographs (Fig. 5 A). For a movement to be counted, the mitochondria were required to fully pass the line. The size of the mitochondria was not considered in the flux calculation. Each kymograph was from a separate neuron and was limited to the first 15 min of observation. Mitochondrial density was calculated from individual frames of time-lapse movies and included both fast-transported and docked mitochondria.

Online supplemental material

Video 1 is a DIC and fluorescent observation of mitochondrial transport during axonal elongation of cultured DRG neurons. Video 2 shows mitochondrial transport during axonal elongation. Video 3 shows mitochondrial transport during a growth cone pause. Online supplemental material is available at http://www.jcb.org/cgi/content/full/jcb.200510097/DC1.

We thank the members of the Sheetz laboratory, Peter Hollenbeck, Davie Van Vactor, our anonymous reviewers, and Steve Heidemann for their helpful discussions, suggestions, careful readings of the paper, and support.

This work was supported by a grant (NS 23345) to M.P. Sheetz from the NIH.

There are no conflicts of interest with the material presented in this paper.

Submitted: 18 October 2005
Accepted: 4 April 2006

References

Abe, I., N. Ochiai, H. Ichimura, A. Tsujino, J. Sun, and Y. Hara. 2004. Internodes can nearly double in length with gradual elongation of the adult rat sciatic nerve. *J. Orthop. Res.* 22:571–577.

Baas, P.W. 1997. Microtubules and axonal growth. *Curr. Opin. Cell Biol.* 9:29–36.

Bae, B.I., H. Xu, S. Igarashi, M. Fujimuro, N. Agrawal, Y. Taya, S.D. Hayward, T.H. Moran, C. Montell, C.A. Ross, et al. 2005. p53 mediates cellular dysfunction and behavioral abnormalities in Huntington's disease. *Neuron*. 47:29–41.

Bamburg, J.R., D. Bray, and K. Chapman. 1986. Assembly of microtubules at the tip of growing axons. *Nature*. 321:788–790.

Bray, D. 1984. Axonal growth in response to experimentally applied mechanical tension. *Dev. Biol.* 102:379–389.

Bridgman, P.C., S. Dave, C.F. Asnes, A.N. Tullio, and R.S. Adelstein. 2001. Myosin IIB is required for growth cone motility. *J. Neurosci.* 21:6159–6169.

Brown, A. 2000. Slow axonal transport: stop and go traffic in the axon. *Nat. Rev. Mol. Cell Biol.* 1:153–156.

Brown, J., and P.C. Bridgman. 2003. Role of myosin II in axon outgrowth. *J. Histochem. Cytochem.* 51:421–428.

Campenot, R.B., and H. Eng. 2000. Protein synthesis in axons and its possible functions. *J. Neurocytol.* 29:793–798.

Campenot, B., K. Lund, and D.L. Senger. 1996. Delivery of newly synthesized tubulin to rapidly growing distal axons of sympathetic neurons in compartmented cultures. *J. Cell Biol.* 135:701–709.

Chada, S.R., and P.J. Hollenbeck. 2004. Nerve growth factor signaling regulates motility and docking of axonal mitochondria. *Curr. Biol.* 14:1272–1276.

Chang, S., V.I. Rodionov, G.G. Borisy, and S.V. Popov. 1998. Transport and turnover of microtubules in frog neurons depend on the pattern of axonal growth. *J. Neurosci.* 18:821–829.

Davis, A.F., and D.A. Clayton. 1996. In situ localization of mitochondrial DNA replication in intact mammalian cells. *J. Cell Biol.* 135:883–893.

Dennerll, T.J., P. Lamoureux, R.E. Buxbaum, and S.R. Heidemann. 1989. The cytomechanics of axonal elongation and retraction. *J. Cell Biol.* 109:3073–3083.

Dent, E.W., and F.B. Gertler. 2003. Cytoskeletal dynamics and transport in growth cone motility and axon guidance. *Neuron*. 40:209–227.

Goldberg, J.L. 2003. How does an axon grow? *Genes Dev.* 17:941–958.

Grafstein, B., and D.S. Forman. 1980. Intracellular transport in neurons. *Physiol. Rev.* 60:1167–1283.

Halloran, M.C., and K. Kalil. 1994. Dynamic behaviors of growth cones extending in the corpus callosum of living cortical brain slices observed with video microscopy. *J. Neurosci.* 14:2161–2177.

Hirokawa, N., S. Terada, T. Funakoshi, and S. Takeda. 1997. Slow axonal transport: the subunit transport model. *Trends Cell Biol.* 7:384–388.

Hollenbeck, P.J., and W.M. Saxton. 2005. The axonal transport of mitochondria. *J. Cell Sci.* 118:5411–5419.

Jay, D.G. 2000. The clutch hypothesis revisited: ascribing the roles of actin-associated proteins in filopodial protrusion in the nerve growth cone. *J. Neurobiol.* 44:114–125.

Joshi, H.C., D. Chu, R.E. Buxbaum, and S.R. Heidemann. 1985. Tension and compression in the cytoskeleton of PC 12 neurites. *J. Cell Biol.* 101:697–705.

Jurado, C., J.R. Haserick, and J. Lee. 2005. Slipping or gripping? Fluorescent speckle microscopy in fish keratocytes reveals two different mechanisms for generating a retrograde flow of actin. *Mol. Biol. Cell*. 16:507–518.

Keith, C.H. 1987. Slow transport of tubulin in the neurites of differentiated PC12 cells. *Science*. 235:337–339.

Lamoureux, P., R.E. Buxbaum, and S.R. Heidemann. 1989. Direct evidence that growth cones pull. *Nature*. 340:159–162.

Lasek, R.J., J.A. Garner, and S.T. Brady. 1984. Axonal transport of the cytoplasmic matrix. *J. Cell Biol.* 99:212s–221s.

Letourneau, P.C., and A.H. Ressler. 1984. Inhibition of neurite initiation and growth by taxol. *J. Cell Biol.* 98:1355–1362.

Letourneau, P.C., T.A. Shattuck, and A.H. Ressler. 1986. Branching of sensory and sympathetic neurites in vitro is inhibited by treatment with taxol. *J. Neurosci.* 6:1912–1917.

Letourneau, P.C., T.A. Shattuck, and A.H. Ressler. 1987. "Pull" and "push" in neurite elongation: observations on the effects of different concentrations of cytochalasin B and taxol. *Cell Motil. Cytoskeleton*. 8:193–209.

Ligon, L.A., and O. Steward. 2000. Movement of mitochondria in the axons and dendrites of cultured hippocampal neurons. *J. Comp. Neurol.* 427:340–350.

Lim, S.S., P.J. Sammak, and G.G. Borisy. 1989. Progressive and spatially differentiated stability of microtubules in developing neuronal cells. *J. Cell Biol.* 109:253–263.

Lim, S.S., K.J. Edson, P.C. Letourneau, and G.G. Borisy. 1990. A test of microtubule translocation during neurite elongation. *J. Cell Biol.* 111:123–130.

Lustbader, J.W., M. Cirilli, C. Lin, H.W. Xu, K. Takuma, N. Wang, C. Caspersen, X. Chen, S. Pollak, M. Chaney, et al. 2004. ABAD directly links Abeta to mitochondrial toxicity in Alzheimer's disease. *Science*. 304:448–452.

Ma, Y., D. Shakiryanova, I. Vardya, and S.V. Popov. 2004. Quantitative analysis of microtubule transport in growing nerve processes. *Curr. Biol.* 14:725–730.

Magnusson, J., M. Orth, P. Lestienne, and J.W. Taanman. 2003. Replication of mitochondrial DNA occurs throughout the mitochondria of cultured human cells. *Exp. Cell Res.* 289:133–142.

Miller, K.E., and H.C. Joshi. 1996. Tubulin transport in neurons. *J. Cell Biol.* 133:1355–1366.

Miller, K.E., and D.C. Samuels. 1997. The axon as a metabolic compartment: protein degradation, transport, and maximum length of an axon. *J. Theor. Biol.* 186:373–379.

Miller, K.E., and M.P. Sheetz. 2004. Axonal mitochondrial transport and potential are correlated. *J. Cell Sci.* 117:2791–2804.

Mitchison, T., and M. Kirschner. 1988. Cytoskeletal dynamics and nerve growth. *Neuron*. 1:761–772.

Morris, R.L., and P.J. Hollenbeck. 1993. The regulation of bidirectional mitochondrial transport is coordinated with axonal outgrowth. *J. Cell Sci.* 104:917–927.

Okabe, S., and N. Hirokawa. 1990. Turnover of fluorescently labelled tubulin and actin in the axon. *Nature*. 343:479–482.

Okabe, S., and N. Hirokawa. 1992. Differential behavior of photoactivated microtubules in growing axons of mouse and frog neurons. *J. Cell Biol.* 117:105–120.

Pfister, B.J., A. Iwata, D.F. Meaney, and D.H. Smith. 2004. Extreme stretch growth of integrated axons. *J. Neurosci.* 24:7978–7983.

Popov, S., A. Brown, and M.M. Poo. 1993. Forward plasma membrane flow in growing nerve processes. *Science*. 259:244–246.

Reinsch, S.S., T.J. Mitchison, and M. Kirschner. 1991. Microtubule polymer assembly and transport during axonal elongation. *J. Cell Biol.* 115:365–379.

Ruthel, G., and P.J. Hollenbeck. 2003. Response of mitochondrial traffic to axon determination and differential branch growth. *J. Neurosci.* 23:8618–8624.

Spero, D.A., and F.J. Roisen. 1985. Neuro-2a neuroblastoma cells form neurites in the presence of taxol and cytochalasin D. *Brain Res.* 355:155–159.

Suter, D.M., and P. Forscher. 2000. Substrate-cytoskeletal coupling as a mechanism for the regulation of growth cone motility and guidance. *J. Neurobiol.* 44:97–113.

Suter, D.M., L.D. Errante, V. Belotserkovsky, and P. Forscher. 1998. The Ig superfamily cell adhesion molecule, apCAM, mediates growth cone steering by substrate–cytoskeletal coupling. *J. Cell Biol.* 141:227–240.

Valente, E.M., P.M. Abou-Sleiman, V. Caputo, M.M. Muqit, K. Harvey, S. Gispert, Z. Ali, D. Del Turco, A.R. Bentivoglio, D.G. Healy, et al. 2004. Hereditary early-onset Parkinson's disease caused by mutations in PINK1. *Science*. 304:1158–1160.

Wagner, O.I., J. Lifshitz, P.A. Janmey, M. Linden, T.K. McIntosh, and J.F. Leterrier. 2003. Mechanisms of mitochondria-neurofilament interactions. *J. Neurosci.* 23:9046–9058.

Zar, J.H. 1999. Biostatistical Analysis. Prentice Hall, Upper Saddler River, NJ. 929 pp.

Zheng, J., R.E. Buxbaum, and S.R. Heidemann. 1993. Investigation of microtubule assembly and organization accompanying tension-induced neurite initiation. *J. Cell Sci.* 104:1239–1250.